# Potentials by inversion of $^3$He + $\alpha$ phase shifts and bound state energies in $^7$Be

S. G. Cooper
*Physics Department, The Open University, Milton Keynes, MK7 6AA United Kingdom*
(Received 10 December 1993)

A method is introduced to determine a potential by inversion from both bound state energies and phase shifts, based upon the iterative perturbative $S$ matrix to potential inversion procedure. The method is applied to determine the local potential reproducing low-energy $^3$He + $\alpha$ phase shifts as well as the $l = 1$ bound states and lowest $l = 3$ resonances in $^7$Be, for both the single channel RGM and empirical data. An even-parity potential is determined from phase shifts up to $l = 4$, which differs significantly from the shape of the odd-parity term. The need for a pronounced parity-dependent potential underlying the RGM is confirmed, which strongly resembles that found in both $\alpha + p$ and $\alpha$ + $^{12}$C scattering.

PACS number(s): 21.60.Gx, 25.10.+s, 25.55.Ci

## I. INTRODUCTION

The elastic scattering and the underlying microscopic description of the $^3$He + $\alpha$ system have been widely studied because of their relevance to the $^3$He$(\alpha,\gamma)^7$Be capture reaction. An accurate theoretical value of the related astrophysical $S$ factor is required for this reaction as an important contribution to the solar neutrino problem. The first microscopic description of the capture reaction based upon the resonating group method (RGM), by Liu, Kanada, and Tang [1], gave a reasonable agreement with the experimental data and this agreement has been improved in further refinements to the theory [2–4]. Some success has also been achieved with descriptions of the $^3$He$(\alpha,\gamma)^7$Be capture reaction based upon local potential models [5–7], where these models are developed to describe experimental properties of the bound state or scattering $^3$He+$\alpha$ system.

In spite of the success of the microscopic description, local potentials still have an important role to play. All microscopic models rely on an accurate representation of the effective nucleon-nucleon force and an inclusion of all relevant multibody interactions. Complex nuclear systems are therefore difficult to describe accurately with such models, whereas descriptions based upon local potentials are considerably easier to formulate and can always be used in a first approximation. The question of particular relevance to this work lies with the determination of the local potential. Usually such potentials are derived either by fitting elastic scattering cross-section data, or by inversion from phase shifts. However, in the context of building a macroscopic model to describe radiative capture, Baye and Descouvemont [8] suggest that the local potential must be able to reproduce both the correct phase shifts and the binding energies of the relevant two-body system. A major purpose of this work is to introduce an extension to the iterative perturbative (IP) $S$ matrix to potential inversion method [9] to allow bound and resonant state energies to be fitted simultaneously with the inversion of phase shifts.

The technique introduced here uses the Born approximation to formulate a corrective term which is added to a potential approximately reproducing the energies of one or more bound or resonant states. This procedure is highly analogous to the use of the Born approximation in the original IP procedure and the new extension is now embodied in the program IMAGO [10]. The Born approximation works well in the calculations presented here and few iterations are required to produce a convergent solution.

The method is applied to derive the local potential which accurately reproduces both the subthreshold $^3$He + $\alpha$ phase shifts and the bound state energies of $^7$Be. The calculations represent the first such direct derivation of the $^3$He + $\alpha$ potential from phase shifts and bound state energies. The main objective of this work is to determine potentials from phase shifts calculated by the single-channel RGM [1, 11], but the determination of potentials from the subthreshold empirical phase shifts is also discussed. Empirical phase shifts for $^3$He + $\alpha$ scattering have been determined over a wide energy range, for example [12–17], both above and below the threshold at $^6$Li + $p$, establishing a fairly clear systematic behavior for individual partial waves as a function of energy. However, in the subthreshold region the uncertainties in the phase shifts are too large to establish a potential accurately by inversion.

The energy dependence of the phase shifts is crucial to IP inversion at subthreshold energies, since there are less than six contributing $l$ values and the potentials are necessarily parity dependent, as predicted by Tang *et al.* [18]. The mixed-case techniques introduced by Cooper and Mackintosh [19] and later extended for mixed-case spin-1/2 scattering [20] are used for the phase-shift inversion. These techniques stabilize the inversion as well as allowing the derivation of an energy-independent potential for a specified energy range. Calculations are also presented to assess the degree of inherent energy dependence in the potentials.

Parity-dependent local potentials have now been established for many nuclear systems, for example, for $p$ + $\alpha$ scattering [20, 21] and for the $\alpha$ + $^{12}$C system [19,

 

22]. In all these cases the even-parity potential is of significantly different shape to the odd-parity potential, whereas most analyses for $^3$He + $\alpha$ scattering [6,7,18] use even- and odd-parity potentials which differ only in the overall potential normalization. Here, the even- and odd-parity potentials are determined in separate calculations. Ambiguities in the odd-parity potential are reduced using the new inversion technique, due to the existence of bound states and subthreshold resonances for odd-$l$ values, whilst ambiguities in the even-parity potential are reduced by the inclusion of partial waves for nonzero $l$ values into the inversion, following Liu *et al.* [5].

The paper is structured as follows: The next section presents the method to fit bound state and resonance energies simultaneously by IP inversion, with a brief example in which potentials are determined to reproduce specifically the lowest $l = 1$ and $l = 3$ states for $^3$He + $\alpha$ and $t + \alpha$ cases. Section III contains a short discussion of the phase shifts used in subsequent calculations, before the separate calculations fitting even-$l$ and odd-$l$ phase shifts are presented in Sec. IV. In Sec. V, comparisons are made with similar systems such as the $n, p + \alpha$ and $\alpha + {}^{12}$C and the underlying parity dependence is discussed before conclusions are presented in Sec. VI.

## II. POTENTIAL INVERSION FROM BOUND STATE ENERGIES

### A. Review of the IP inversion method

The details of the iterative perturbative inversion procedure have been described in many previous articles [9, 19] and references therein, with the "Users manual for the code IMAGO" [10] providing a comprehensive and up-to-date account. Only the essentials of the method will be repeated here, in order to show how the extension to fit bound state energies is accommodated within the existing procedure.

First a potential must be chosen as the starting reference potential (SRP), $V_{\rm SRP}(r)$. This potential should be a reasonable approximation to the (unknown) target potential, although in many cases the spin-orbit component, and sometimes also the central component, may be zero.

A potential perturbation is formed from an expansion over a finite set of basis functions, $v_i(r)$, i.e.,

$$V_{\rm inv}(r) = V_{\rm SRP}(r) + \sum_i \lambda_i v_i(r), \tag{1}$$

where the optimum expansion coefficients, $\lambda_i$ are determined by the inversion. The accuracy of the phase-shift fit at any stage of the inversion is measured by the "phase-shift distance" $\sigma^2$, given by

$$\sigma^2 = \sum_{k=1}^{N_k} \left| S_k^{\rm tar} - S_k^{\rm inv} \right|^2, \tag{2}$$

where $k$ is a generalized partial wave index specifying $l$, $j$ (for spin half), and, in mixed-case inversion, $E$, the c.m. energy. $S_k^{\rm tar}$ is the target $S$ matrix to be fit by the inversion and $S_k^{\rm inv}$ is the $S$ matrix resulting from solving the radial Schrödinger equation for $V_{\rm inv}$ (or initially $V_{\rm SRP}$).

The essential step in the method is the assumption of a linear relation between small changes in the $S_k^{\rm inv}$ and small values of $\lambda_i$, following the Born approximation

$$\delta S_{ki} = \lambda_i \left( -\frac{im}{\hbar^2 k_s} \right) \int_0^\infty v_i(r) \left[ u_k(r) \right]^2 \, dr, \tag{3}$$

where $u_k(r)$ is the suitably normalized radial wave function obtained by solving Schrödinger's equation for $V_{\rm SRP}(r)$ [initially; later $V_{\rm inv}(r)$] and $k_s$ is the usual asymptotic wave number, $= \sqrt{(2\mu E)}$ for reduced mass $\mu$. A least squares minimization of $\sigma^2$ produces a set of linear equations for the $\lambda_i$ and the matrix inversion is solved using singular value decomposition (SVD). The phase shifts show a greater sensitivity to certain basis functions, or in practice to particular linear combinations of the basis set. The linear combination producing least sensitivity corresponds to the smallest singular values in the decomposed matrix, so that by removing these singular values from the calculation of the set of $\lambda_i$, a divergent solution can be avoided [23]. The insertion of the $\lambda_i$ into Eq. (1) then produces a new potential $V_{\rm inv}(r)$ corresponding to an decreased value of $\sigma^2$. The whole process can then be repeated until the convergence in $\sigma^2$ is satisfactory. Typically for nucleon scattering this takes $< 5$ iterations and sometimes two iterations are sufficient.

The choice of both $V_{\rm SRP}(r)$ and the basis functions $v_i(r)$ necessarily introduces some degree of parameter dependence into the IP procedure, which may lead to significant uncertainties in the final potential if the inversion basis is small. This parameter dependence can be assessed by further calculations based upon alternative choices of $V_{\rm SRP}(r)$ and $v_i(r)$ (for example, the basis could be formed from either zeroth-order Bessel functions or Gaussian functions). The sensitivity of the potentials to small changes can also be found by notch testing. In this procedure, a small Gaussian notch is added to $V_{\rm inv}(r)$ and the change in sigma is calculated as a function of the position of the notch center.

A key advantage of the IP method lies in its simplicity, allowing easy generalization to more complex scattering cases. For example, Eq. (1) can be adapted to derive imaginary and/or spin-orbit potentials where appropriate and known errors in the target $S$ matrix can be translated into suitable weighting in Eq. (2) [9], where relevant. Similarly, Eq. (2) can include $S$-matrix elements for more than one energy and subsets of the elements $S_k^{\rm tar}$ can be excluded from the inversion. In heavy-ion scattering it may be essential to exclude small $l$ values from the inversion, because they do not contribute strongly to the cross section and may result from an underlying highly $l$-dependent potential whose radial form is not of interest [23]. More relevantly here, a parity-dependent potential can be determined by excluding either all the odd-$l$ or all the even-$l$ values in two independent inversion calculations. In mixed-case inversion phase shifts corresponding to more than one energy are included. By using a parametrized form for the phase shifts, the inversion can be restricted to energies within a very narrow

range, i.e., an "energy bite" [20], so that, effectively, the energy derivatives of the phase shifts are used to calculate an essentially energy-dependent potential.

### B. Bound state inversion procedure

The extension of the IP inversion procedure to include the inversion from bound or resonance state energies is based upon the standard iterative procedure to calculate a single-particle bound state of angular momentum $l$. The latter procedure has been widely used for many years to represent single-particle form factors in stripping codes such as DWUCK, [24] and has been extended to calculate resonant states in the distorted wave Born approximation (DWBA) by Comfort [25]. Cooper *et al.* [26] showed how states of near zero, or even zero energy can be calculated with suitable low-energy approximations for the Coulomb functions.

The procedure for calculating either a bound state or a low-energy resonance is as follows: For some initial choice of potential, e.g., $V_{\rm SRP}(r)$, solutions to the radial Schrödinger equation are calculated for the radial regions inside and outside a suitable matching radius $R_m$. In the external region the solution $\phi_2(r)$ is computed working radially inwards, starting from the Coulomb function $O_l^-(\mathrm{R})$ or $G_l(R)$ for the bound and resonant state solutions, respectively, at a radius $R \gg R_m$, where the nuclear potential is negligible. In the internal region, the solution $\phi_1(r)$ is evaluated working radially outwards from an arbitrary value at the first radial point. [While in most calculations the wave function is assumed to behave as $r^{l+1}$, near $r = 0$, an approximation valid if the nuclear potential is independent of radius for small $r$, by setting $\phi_1(0) = 0$ and using the Numerov method of integration no such assumptions need be made near $r = 0$.] The solution $\phi_1(r)$ should contain the required number of radial nodes. At $r = R_m$ the difference between the logarithmic derivatives of the two functions is evaluated and, as for an arbitrary choice of potential and energy, a bound state or resonance will not exist, the two logarithmic derivatives will differ. Either the potential must be adjusted to reproduce the specified energy or the energy adjusted to find the appropriate state for given $V_{\rm SRP}$.

An improved approximation to $V_{\rm SRP}$ can be obtained by adding to this potential a single basis function $\lambda_i v_i(r)$ and then applying the Born approximation to solve for $\lambda_i$, i.e.,

$$\lambda_i \left\{ \frac{1}{[\phi_1(R_m)]^2} \int_0^{R_m} v_i(r)[\phi_1(r)]^2 dr + \frac{1}{[\phi_2(R_m)]^2} \int_{R_m}^{R} v_i(r)[\phi_2(r)]^2 dr \right\} = \left( \frac{\phi_2'}{\phi_2} - \frac{\phi_1'}{\phi_1} \right)_{r=R_m} . \tag{4}$$

The complete procedure can now be repeated on an iterative process, with each successive stage starting from the potential calculated at each previous step, until the state energy is reproduced to satisfactory precision. In most codes the overall potential depth, or, for spin-1/2 states, the sum of central and spin-orbit potentials, is adjusted using this procedure.

Where several bound state and/or resonance energies are now to be reproduced simultaneously, a larger potential basis can be used, as in IP phase shift to potential inversion. To combine this new method with the phase-shift inversion, consider a minimization of the following quantity:

$$\sigma'^2 = \sigma^2 + W^2 \sum_n \left( \frac{2}{k_n} \right)^2 \left| \frac{\phi_2'^n}{\phi_2^n} - \frac{\phi_1'^n}{\phi_1^n} \right|^2_{r=R_m} . \tag{5}$$

$\sigma^2$ is as before, Eq. (2), and the second sum on the right hand side (RHS) is over a set of bound states or resonances; for each state $n$, $\phi_1^n(r)$ and $\phi_2^n(r)$ represent the internal and external solutions as described above, and $k_n$ is the asymptotic wave number. The adjustable factor $W^2$ introduces a bias between a precise fitting of phase shifts and a precise fitting of the energies of the states $n$. The factor $2/k_n$ is inserted only to give a closer correspondence between the two terms on the RHS of Eq. (5), i.e., so that the two approximations in Eqs. (3) and (4) have roughly equal weight in the inversion matrix if $W \sim 1$.

The quantity $\sigma'^2$ can be minimized by the least squares method, using the approximations given by Eqs. (4) and (3). The introduction of the second term on the RHS of Eq. (5) introduces additional equations which govern the fitting of the single-particle states. SVD techniques described in Sec. II A are used here and the complete process can be iterated until $\sigma'^2$ converges.

In the following sections, the original measure $\sigma^2$ is used to specify the fit to the phase shifts and the actual energies of each state $n$ are calculated separately, rather than directly quoting the value of $\sigma'^2$ for any calculated potential $V_{\rm inv}(r)$. The calculation of the state energies corresponding to $V_{\rm inv}(r)$ follows a procedure similar to that based upon Eq. (4). For each state $n$, solutions $\phi_1^n(r)$ and $\phi_2^n(r)$ are calculated using the Schrödinger equation with the potential $V_{\rm inv}(r)$ and, initially, the target energy. A correction $(\delta k^2)_n$ to the state energy is calculated using the Born approximation and the whole calculation is repeated iteratively until the two solutions $\phi_1^n$ and $\phi_2^n$ match at the radius $R_m$.

The code IMAGO has been adapted to include the new techniques within inversion calculations. Since bound states and resonances are treated on an equal footing, the procedure can include cases in which $V_{\rm SRP}(r)$ has an unbound state although a bound state is required experimentally, or vice versa. However, if $\phi_1^n(r)$ contains the incorrect number of nodes, an appropriate potential correction will not be found by inversion and an improved choice of $V_{\rm SRP}$ is required.

### C. Inversion from bound and resonance states only in $^3$He/$t$ + $\alpha$

The method introduced in Sec. II B will first be illustrated with inversion calculations based upon the bound and resonant state energies alone [in practice Eq. (5) is

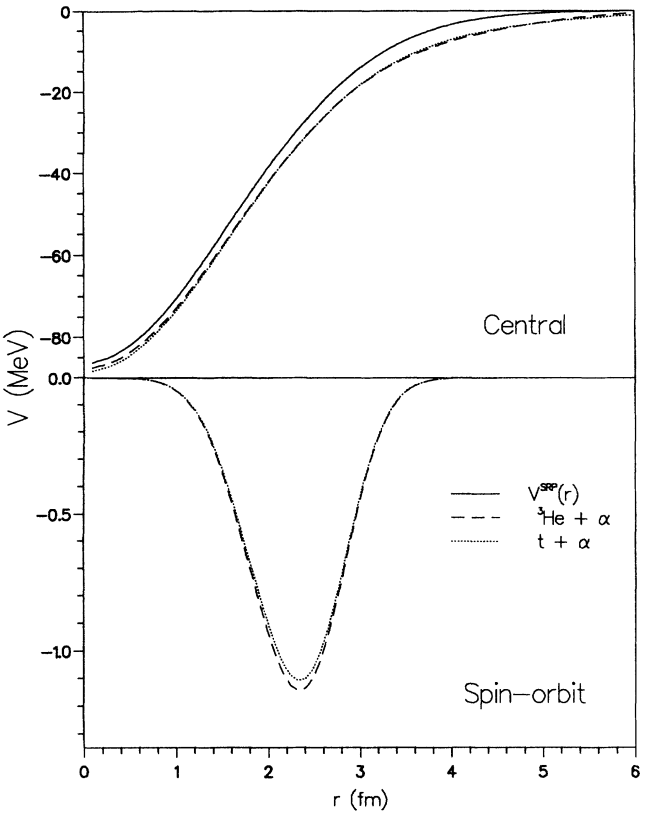


FIG. 1. Central and spin-orbit potentials determined by inversion of the bound states and lowest $F$-wave resonances in $^7$Be (dashed line) and $^7$Li (dotted line), and compared with the starting reference potential $V_{\rm SRP}$ (solid line).

used with a large weighting factor $W$], before combining the methods in Secs. II A and II B to calculate a potential simultaneously fitting bound states and phase shifts. In past analyses a more *ad hoc* procedure has been used to determine potentials which approximately reproduce several single-particle energies simultaneously, for example, by adjusting the parameters of a fixed shape potential. By using direct inversion from the bound or resonance energies, no fixed potential shape need be assumed, although the accuracy of the resulting potential is necessarily restricted by the number of states included in the inversion. The example considered here is based on the $l = 1$ bound states and the lowest $l = 3$ resonance states in $^3$He + $\alpha$ and $t + \alpha$ scattering.

The form of $V_{\rm SRP}(r)$ used was deliberately chosen to be inaccurate, i.e., in all cases predicting energies which are too high and giving positive energies for even the lowest $l = 1$ states. The inversion is based upon a central potential basis of three Gaussians and a spin-orbit basis of two Gaussians, with which to fit four bound state or resonance energies. The inversion matrix is then underdetermined, but by using SVD techniques only three linear combinations of these basis functions are used at any iteration and the inversion converges well within five iterations.

The separation of the $l = 1$ states in $^7$Be remains difficult to reproduce. An accurate fitting of these bound state energies is only obtained either by using a spin-orbit basis comprising of two relatively narrow width Gaussians (of width = 0.6 fm and spaced at 1.9 and 2.5 fm), or by allowing an oscillation in the spin-orbit potential. Buck *et al.* [6] were also unable to reproduce the $P$ and the $F$ state energies simultaneously with a single Gaussian spin-orbit potential. However, beyond experimenting with the position of the two spin-orbit basis functions in the inversion, no further attempts have been made to vary the choice and size of the bases to optimize the fit. With the $V_{\rm SRP}(r)$ used for the $^3$He + $\alpha$ states, including the spin-orbit basis comprising the narrow width Gaussians, the lowest $P$ and $F$ states in the $t + \alpha$ system are also reproduced accurately. Calculations with slightly different spin-orbit bases do suggest that the $^7$Li states could be fit better with a spin-orbit potential of wider width and the $^7$Be states better fit with a spin-orbit potential of narrower width and this observation may reflect state mixing in one or both of the cases.

Figure 1 shows the resulting potentials for both $^3$He + $\alpha$ and $t + \alpha$ cases, with the rather sharply peaked spin-orbit potentials, as well as $V_{\rm SRP}(r)$ as used in these calculations, which has effectively a zero spin-orbit component. The two solutions show a remarkable agreement, even in the spin-orbit potential, and perhaps rather better than expected given the probable presence of some degree of state mixing. The energies obtained for each state $n$ from these two solutions are given in Table I and agree with the experimental values to within 0.1 MeV. With the small expansion basis the solutions are necessarily parameter dependent and therefore not unique. However, since the solutions are very smooth, alternative solutions are likely to contain potential oscillations.

The above calculations are essential to calculate a $V_{\rm SRP}(r)$ for the phase shift inversion in $^3$He + $\alpha$ scattering. With an arbitrary choice of $V_{\rm SRP}(r)$, problems arise in the original IP procedure because the linearity rela-

TABLE I. For the lowest odd-$l$ states in $t + \alpha$ and $^3$He + $\alpha$, experimental energies $E_{expt}$, and energies $E_{inv}$ and $E_{SRP}$, calculated, respectively, for the potentials $V_{inv}(r)$ and $V_{SRP}(r)$. All energies are in MeV.

| | $^7$Be | | | $^7$Li | | |
|---|---|---|---|---|---|---|
| State | $E_{expt}$ | $E_{invs}$ | $E_{SRP}$ | $E_{expt}$ | $E_{invs}$ | $E_{SRP}$ |
| $P_{1/2}$ | -1.159 | -1.143 | 1.90 | -1.991 | -1.981 | 1.365 |
| $P_{3/2}$ | -1.588 | -1.607 | 1.90 | -2.468 | -2.479 | 1.365 |
| $F_{5/2}$ | 5.14 | 5.09 | 8.70 | 4.211 | 4.199 | 7.565 |
| $F_{7/2}$ | 2.98 | 2.99 | 8.70 | 2.162 | 2.165 | 7.565 |

tionship, Eq. (3), breaks down in the region of narrow resonances, such as the $F_{7/2}$ resonance at the excitation energy of 4.57 MeV. By first fitting the resonance energy directly using Eq. (4), the inversion works well.

## III. PHASE-SHIFT DATA

Only real phase shifts are included here, with which to determine real central and spin-orbit potentials. The empirical phase shifts for the subthreshold energy region [12–14] are only well established for the $S$-, $P$-, and $F$-wave phase shifts (in cases where the $D$-wave phase shifts were allowed to vary [12, 14], no significant departures from zero were found). The threshold for breakup to $^6$Li + $p$ is at 5.608 MeV excitation energy (corresponding to 7.036 MeV for the $^3$He projectile), but just above threshold the empirical values of $\eta = |S(l)|$ are still close to unity. Hence although inversions will be presented for laboratory energies up to 12 MeV, the neglected small changes in $\eta$ should not effect the real potentials.

The single-channel RGM calculations contain the freedom to fine-tune the nucleon-nucleon potential to fit appropriate experimentally established properties. For example, the lowest $F$-wave resonance energies are accurately positioned to calculate bremsstrahlung cross-sections [11], now referred to as LTK1, or in [1], to be denoted LKT2, the $^7$Be bound state energies are accurately fitted in order to calculate the $^3$He$(\alpha,\gamma)^7$Be capture reaction. The inversions will be mostly based on the phase shifts given by LTK1. The RGM analyses have not used prior information concerning the even $l$ phase shifts and all the one-channel RGM calculations produce $S$-wave phase shifts which differ significantly from the empirical values. This discrepancy is only corrected by the inclusion of specific distortion effects [27]. The empirical data are not sufficiently precise to permit judgement on the RGM $D$-wave phase shifts, and the RGM $G$-wave phase shifts are very small in the subthreshold energy region (in LTK1 negative $G$-wave phase shifts are given, probably due to accurately fitting the $F$-wave resonances). To ensure a continuity to higher energies, the potential models must give reasonable phase shifts for $l = 4$ and some inversions have included $G$-wave phase shifts calculated from the $R$-matrix fits of Furber *et al.* [28]. The latter fits are based upon calculations extending up to 113 MeV (c.m.) and include predictions for $G$- and $H$-wave resonances which have been approximately justified by the empirical phase shift fits of Ostashko and Yasnogorodskii [17].

To allow an unrestricted choice of energies in the phase shift to potential inversion, the RGM phase shifts have been fitted with either effective range parametrizations, or, for the $D$-wave phase shifts only, $R$ matrix fits. This fitting process was made separately for each partial wave, with an objective to obtain fits to the RGM phase shifts of greater accuracy than is generally achieved by inversion, as opposed to deriving meaningful fitting parameters.

The empirical phase shifts are too scattered to provide an accurate basis for inversion and serve only to restrict the possible shape of the underlying local potential. The empirical $S$-wave phase shifts are reasonably well approximated by the hard sphere model [12], which is used to assess potential differences between fitting the RGM and fitting empirical phase shifts.

## IV. RESULTS OF INVERSION CALCULATIONS

### A. Inversion parameters

Generally the inversion calculations are fairly insensitive to the choice of $V_{\rm SRP}(r)$. However the spin-orbit potential presents a challenge to the inversion because, in all cases, it is an order of magnitude or more smaller than the central potential. Most calculations start with a zero spin-orbit potential, and perturbations are added to the spin-orbit potential only after first determining a good approximation for the central potential. Correspondingly, as a fraction of the potential value, the uncertainties in the final spin-orbit potential are much larger than for the central component. A small Gaussian basis is generally used.

The IP approximation of Eq. (3) works well in the following calculations except near the $F_{7/2}$ resonance as discussed in Sec. II C. The simple smoothing techniques, introduced in Ref. [20], have been used in some calculations to remove long-range surface oscillations. Usually, such oscillations can also be removed by restricting the radial range of the inversion basis.

The Coulomb potential used is given by $4e^2/r\,\mathrm{erf}(\beta r)$ as obtained from the RGM calculations [5, 29], with $\beta = 0.552$.

### B. Odd-parity potential

In this section, local potentials are presented, calculated to reproduce both the phase shifts of LTK1 and the bound state energies. While the bound state energies given by LTK1, $-1.09$ and $-1.95$ MeV for the $P_{1/2}$ and $P_{3/2}$ states, respectively [30], differ slightly from the experimental values, the inversion must be based on the actual energies given by the RGM. Otherwise there is an inevitable compromise between accurately reproducing the bound state energies and precisely fitting the energy dependence of the phase shifts.

The inversion procedure is most stable when performed in several stages; first, only the bound state and resonance energies are included in the calculation, as in Sec. II C, and an accurate fit to these energies is obtained. Subsequently the weighting factor $W$ is decreased in one or more stages to $\sim 1$ (but with even-$l$ phase shifts excluded from $\sigma^2$) and the inversion basis enlarged, so that the overall phase shift fit is gradually improved whilst a good fit to the bound state energies is maintained. The RGM bound state and resonance energies alone can be very precisely reproduced with a Gaussian spin-orbit potential of greater width than that presented in Sec. II C. The resulting potential provides a reasonable fit to the odd-parity phase shifts, although the fit to the $P$-wave phase shifts becomes less accurate towards higher energies.

In Fig. 2, the potential obtained from fitting only the bound and resonance state energies (solid line) is compared with three potentials resulting from full inversion calculations, for which $\sigma = 0.108$, 0.117, and 0.109. The latter potentials are calculated using different choices for both $V^{\mathrm{SRP}}$ and the inversion parameters and are determined from inversion of phase shifts for energies up to 12 MeV (in steps of 0.5 MeV) to cover the $F_{5/2}$ resonance. All the potentials shown in Fig. 2 reproduce bound and resonance state energies to within 0.1 MeV. In this same energy range, the potential inverted from the single-particle states alone gives $\sigma = 1.15$. However, only small changes to the latter potential are required to reproduce the full energy dependence of the phase shifts accurately and the resulting solutions do not reveal a significant parameter dependence. Differences between the central potentials shown in Fig. 2 are noticeable only for small radii and notch tests show that even the $P$-wave phase shifts show little sensitivity to this radial region. The comparative differences in the spin-orbit potentials are proportionally larger due to the much smaller magnitude. The differences between the phase shifts calculated from any one of the three solutions in Fig. 2 and the parametrized RGM odd-$l$ phase shifts are $< 1^\circ$ for the entire energy range. Comparable fits to the phase shifts can be obtained if the bound state energies are excluded from the inversion, but the resulting spin-orbit potentials have significantly larger uncertainties than is illustrated by the range of solutions in Fig. 2.

If the inversion is restricted to subthreshold energies, the accuracy of the calculations is slightly improved, but any changes to the potentials fall well within the uncertainties due to the parameter dependence as illustrated in Fig. 2. Any underlying energy dependence in the potential should be small and this prediction is confirmed by calculations in which the phase shifts are fitted very precisely at energy bites centered at 2, 4, and 6 MeV. The resulting three potentials, including the spin-orbit components, show only very small differences from the potential determined by inversion from the full subthreshold energy range.

Phase shifts and bound state energies from other RGM calculations can also be easily fitted by inversion, yielding calculations of similar accuracy to those reported above. Figure 3 compares a potential determined by inversion from the subthreshold odd-$l$ phase shifts of LTK1 with a potential similarly determined from the phase shifts of LKT2. The two models give slightly different predictions for the $P$-wave phase shifts and very different predictions for the centroid of the $F$-wave resonances. The largest differences in the equivalent local potentials are found in the relative magnitude of the spin-orbit potential, with

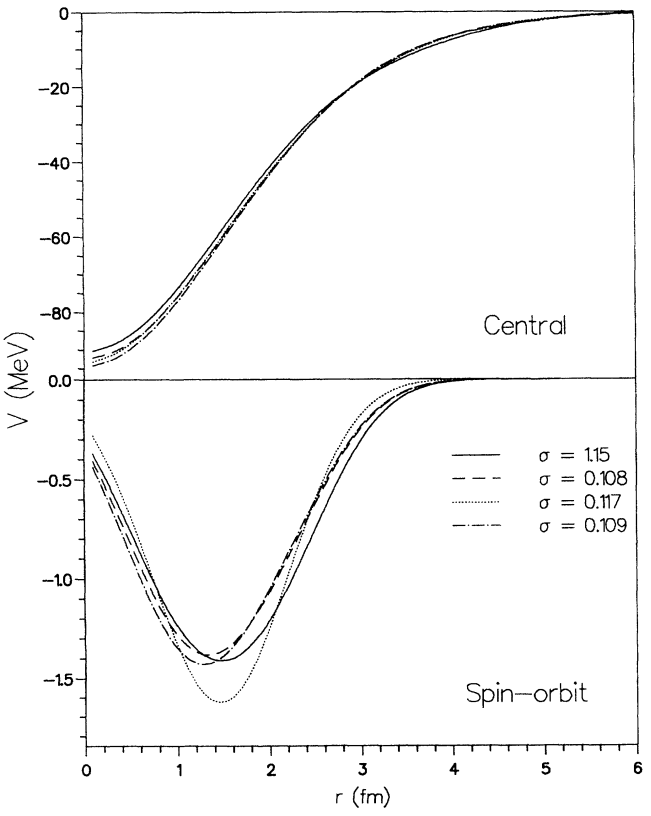


FIG. 2. Central and spin-orbit potentials for $^3$He + $\alpha$ (i) determined by inversion of the bound and resonance state energies only, giving $\sigma = 1.14$ (solid line), and (ii) in three separate calculations, determined to reproduce both the odd-$l$ phase shifts and the bound state energies, giving $\sigma = 0.108$ (dashed line), $\sigma = 0.117$ (dotted line), or $\sigma = 0.109$ (dash-dotted line).

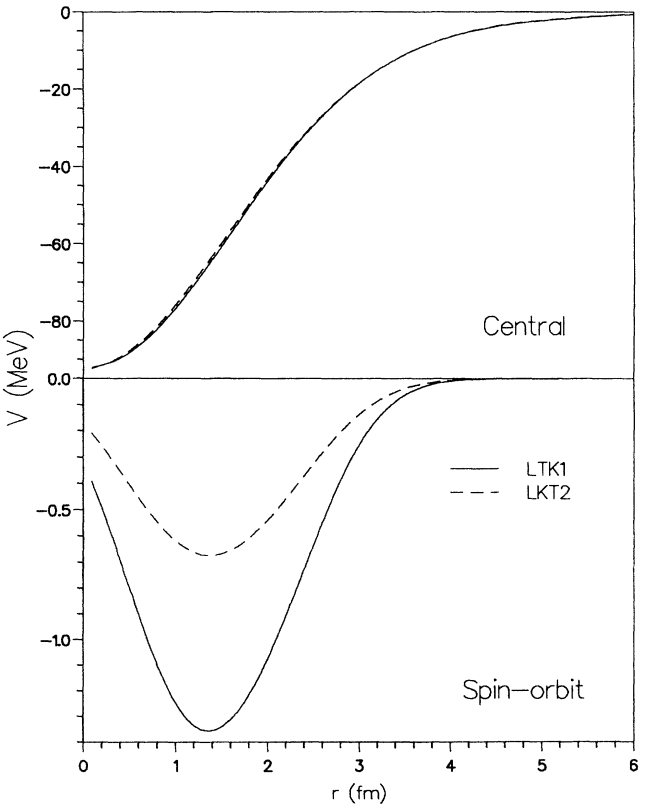


FIG. 3. Central and spin-orbit odd-parity potentials locally equivalent to two RGM analyses of $^3$He + $\alpha$, LTK1 (solid line) and LKT2 (dashed line).

only very small corrections required in the central potential to adjust the centroid of the resonances.

The inversion procedure can also determine a potential from the empirical phase shifts and experimental bound state energies, whilst retaining the narrow spin-orbit potential. The resulting central potentials are very similar to those given in Fig. 2. Since accurate fitting of the phase shifts entails reproducing the experimental noise, it is unclear whether the very narrow spin-orbit potential is required to reproduce the empirical phase shifts accurately.

### C. Even-parity potential

The inversion on even-$l$ values is rather less straightforward than that on odd-$l$ partial waves. No even-$l$ bound states exist, although putting $^3$He + $\alpha$ in a common oscillator potential gives rise to Pauli forbidden states in both $S$ and $D$ waves. By specifically excluding these forbidden states, the potential solution can be restricted to lie within that family of solutions which contain the correct number of wave function nodes.

The subthreshold $S$-wave phase shifts alone are extremely easy to fit. A series of calculations have been made using Gaussian central potentials with fixed width, 1.6, 2.0, or 2.4 fm, and with the depths varied to reproduce the $S$-wave phase shifts of LTK1 accurately up to 12 MeV (laboratory). In Fig. 4 the $D$- and $G$-wave phase shifts calculated from the resulting potentials are compared with the appropriate RGM phase shifts (solid line). Clearly the higher $l$ values are fit much better with the Gaussian potentials of smallest width. In fact, while the $G$-wave phase shifts may be too small to be fitted accurately by inversion, the calculations of Furber *et al.* [28] imply that at 12 MeV, $\delta < 1°$. Notch tests on the resulting potentials reveal a strong association between the $l$ value and the radial region of greatest sensitivity; i.e., the $S$ wave is most sensitive to radial regions near 0 fm and near 2 fm, the $D$ wave is most sensitive to $r \sim 1$–2 fm, and the $G$ wave shows a much smaller sensitivity which is strongest for radii $r \sim 3$–4 fm.

Starting from the single Gaussian central potential derived above with a width of 1.6 fm, the fit to all subthreshold energies phase shifts is slightly improved, in a second inversion stage, using a larger inversion basis as well as a spin-orbit potential. The two separate stages are necessary to give a stable inversion. The phase shifts corresponding to the improved potential are compared with the parametrized RGM phase shifts in Fig. 5, for both the $S$- and $D$-wave phase shifts. Note that the $D$-wave phase shifts are still less than 2.5° in this energy region. The final potential is shown in Fig. 6 (solid line) and discussed below. Whilst the two sets of phase shifts in Fig. 5 show a more noticeable disagreement at higher energies, the new solution presents a significant improvement on the approximate local potentials suggested by Liu *et al.* [5].

To improve the accuracy of the subthreshold phase shifts fits beyond the agreement illustrated in Fig. 5 requires either pronounced oscillations, or energy-dependence, to be introduced into the potential. As in Sec. IV B, the energy dependence is investigated by calculating potentials for energy bites centered at 2, 4, and 6 MeV with widths ±0.4 MeV. The potentials determined from inversion of all subthreshold phase shifts is used for $V_{\rm SRP}(r)$, to ensure a continuity with energy, and the inversion basis is restricted to $r < 3$ fm, to both maintain a reasonable fit to the $G$-wave phase shifts and also to restrict the parameter dependence of the potentials. The energy-dependent solutions fit the $S$- and $D$-wave phase shifts extremely accurately in the region of each energy bite. The potentials are shown in Fig. 6, along with the solution for the complete subthreshold energy range. As in the odd-parity case, the central potential contains little energy dependence, and only small corrections need be added to the potentials to fit the $S$-wave phase shifts accurately for each energy bite. The proportionally much larger changes required in the spin-orbit potentials explains why the inversion covering the wider energy range fails to reproduce the energy dependence of the $D$-wave phase shifts.

A similar form of energy dependence to that reported in the preceding paragraph is obtained for inversions from the phase shifts of LKT2, which is not surprising as the two models do not give significantly different results for

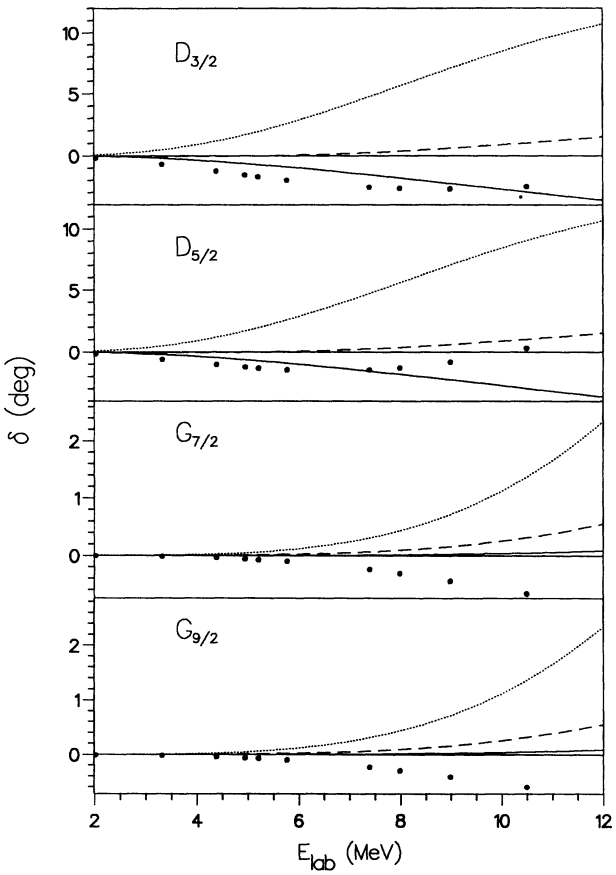


FIG. 4. $D$- and $G$-wave phase shifts, plotted as a function of energy, for Gaussian potentials of widths 1.6 fm (solid line), 2.0 fm (dashed line), and 2.4 fm (dotted line) compared with published RGM phase shifts of LTK1 (solid circles).

the $S$- and $D$-wave phase shifts. However, the differences between the two potentials determined by inversion from the subthreshold phase shifts of LTK1 or LKT2 are very similar to the differences found between the solutions determined from the two models for the odd-parity case, as shown in Fig. 3. That is, the two central potentials show an almost perfect agreement, whilst a much smaller spin-orbit potential is required to fit the phase shifts of LKT2 than for LTK1. (The volume integrals and rms radii of the two potentials are tabulated in Table II and discussed in Sec. V B below.)

Large ambiguity problems are found if the empirical $S$-wave phase shifts are fitted with the single Gaussian central potentials considered above, but the resulting potentials have less attraction than the potential determined from the RGM. However, negative $D$-wave phase shifts are obtained in the subthreshold energy region for all choices of the Gaussian width. Negative $D$-wave phase shifts are both predicted by RGM calculations, with and without specific distortion effects, and justified to some extent by the empirical phase shifts. The Gaussian potential with width 2.4 fm is incorrect if the $G$-wave phase shifts are less than 1° at 12 MeV, as suggested by empirical analyses at higher energies. When the $G$-wave phase shifts are included within the phase-shift analyses, the variations from zero remained less than 2° at 18 MeV (laboratory) [12]. Also, $R$-matrix fits have been made to the established $9/2^+$ resonance, higher in energy than the range considered here [17], which imply even smaller phase-shift values in the subthreshold energy region. Only small adjustments in the potential are required to reproduce both $S$- and $D$-wave phase shifts simultaneously, if the potential solution is based on the Gaussian with smaller width. The even-parity potential is therefore poorly determined by the empirical phase shifts, but reasonable restrictions on the potential, imposed to fit the $G$-wave phase shifts, still lead to an even-parity potential of significantly decreased radial extent than that of the odd-parity potential (which can be well approximated by a Gaussian of width 2.4 fm). The empirical phase shifts at least partially confirm the shape of the even-parity potential derived from the one-channel RGM.

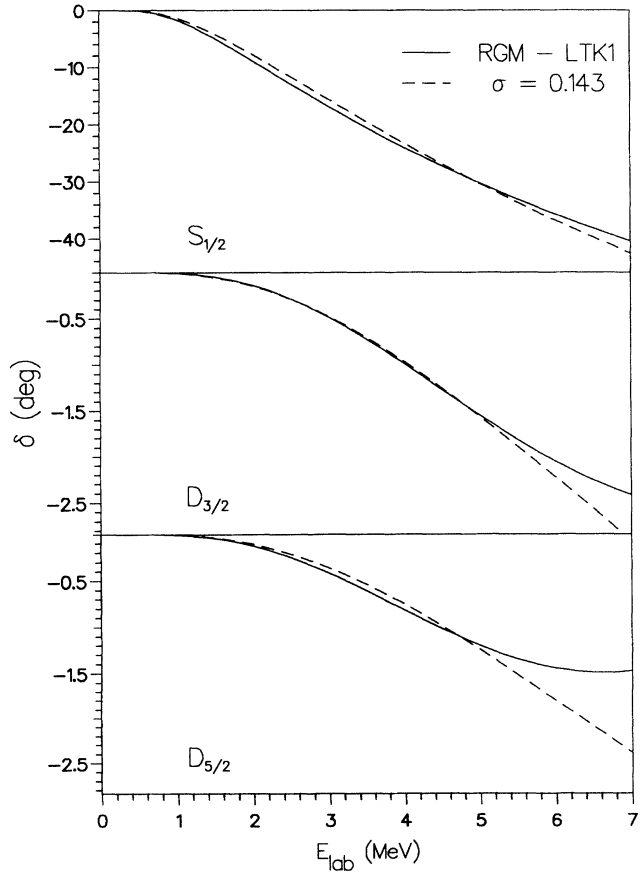


FIG. 5. $S$- and $D$-wave phase shifts, plotted as a function of energy, for the RGM phase shifts, LTK1 (solid line), and phase shifts corresponding to the best smooth potential determined by inversion from subthreshold phase shifts of LTK1 (dashed line).

## V. COMPARISON WITH OTHER NUCLEI

### A. Even-parity potential

Since the evidence from the empirical phase shifts is insufficient to confirm the shape of the even-parity po-

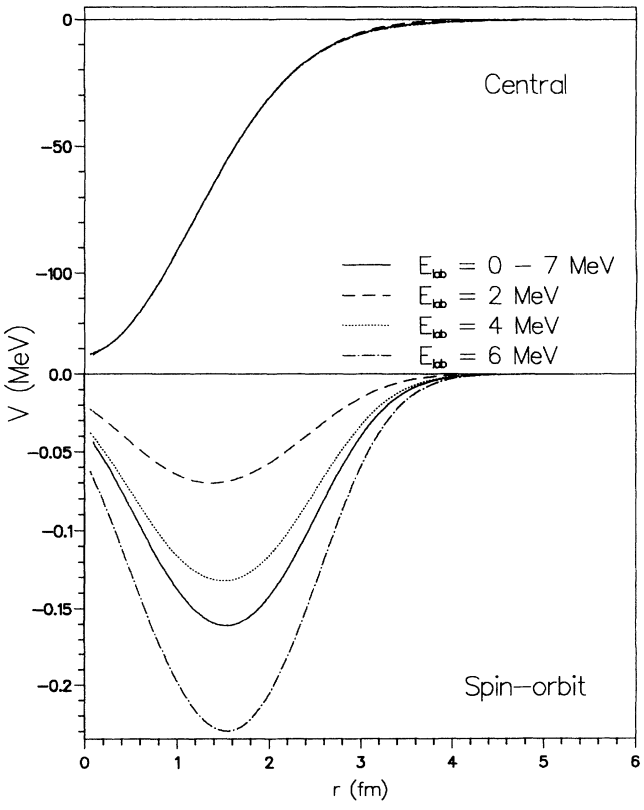


FIG. 6. Central and spin-orbit even-parity potentials determined from phase shifts covering (i) the complete subthreshold energy range (solid line), and (ii) energy bites centered at 2 MeV (dashed line), 4 MeV (dotted line), and 6 MeV (dash-dotted line).

tential deduced from the one-channel RGM, it is interesting to investigate the systematics between various nuclei for this potential. In Fig. 7 the even-parity potential determined by inversion over the complete subthreshold region, i.e., the solid line in Fig. 6, is compared with the even-parity $p+\alpha$ potential determined from RGM phase shifts for an energy bite of 12 MeV [21] and the potential fitting the single-channel $\alpha+\alpha$ RGM phase shifts of Liu [31]. The latter potential is close to the two-Gaussian equivalent local potential proposed by Liu, but has now been modified by IP inversion to reproduce all the subthreshold RGM phase shifts accurately up to $l = 6$. For $\alpha+\alpha$ scattering the small differences between the single-channel RGM phase shifts and the empirical phase shifts should not be important and the $\alpha+\alpha$ potential displayed in Fig. 7 is very similar to the potential obtained by Buck *et al.* to fit the empirical phase shifts [32]. The close correspondence between all three systems suggests a consistent pattern for the potential separately fitting even-$l$ phase shifts in this mass region. Possibly the $^3$He + $\alpha$ potential is not quite in line with other cases; i.e., the rms radius may be too small, so that the omissions in the single-channel RGM may be exaggerating the shape of the $^3$He + $\alpha$ potential.

### B. Parity-dependent potential

A parity-dependent potential of the form $V_1(r) + (-1)^l V_2(r)$ can be calculated from the odd- and even-parity potentials. Only the central potentials are considered here, so that the effects of both energy dependence and the sensitivity to inversion parameters should not affect the shape of the resulting parity-dependent potential. Potentials $V_1(r)$ and $V_2(r)$ corresponding to the potentials determined from the subthreshold phase shifts and the bound state energies of LTK1 are shown in Fig. 8. The $p$ + $\alpha$ parity-dependent potentials determined from both empirical phase shifts [20] and RGM phase shifts [21] in both cases for an energy bite at 12 MeV, and the parity-dependent potentials fitted to subthreshold $\alpha$ + $^{12}$C phase shifts [19] are also shown in Fig. 8. In all systems the parity dependence is far from a simple renormalization of either the even- or odd-parity potential. The parity-independent term is smooth in all cases and increases in magnitude in an approximately systematic way with the mass of the target and projectile. By contrast, the parity-dependent terms $V_2(r)$ contain positive and negative regions, but there is a quite remarkable similarity in the shape and magnitude for the different cases. In all cases the magnitude of $V_2(r)$ is smaller, but far from insignificant, in comparison with $V_1(r)$.

The volume integrals per nucleon, $J$, as usually defined, and rms radii for both the even and odd-parity potentials, locally equivalent to LTK1, and the values for the average potential $V_1(r)$ are listed in Table II, which also includes, for completeness, the values for the potentials determined from the phase shifts of LKT2. Whilst the large differences between the rms radii of the odd- and even-parity central potentials can be expected from Figs. 2 and 6, the very large differences in the corresponding volume integrals may seem surprising. However, it is the values for the parity-independent term which should be compared with the systematics for heavier nuclei. There is also the expected close correspondence in the volume integrals and rms radii of the central

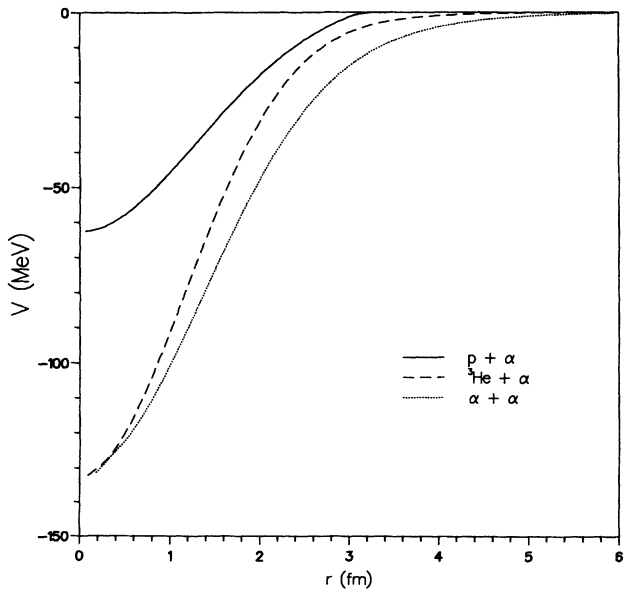


FIG. 7. Central even-parity potentials for $p$ + $\alpha$ (solid line), $^3$He+$\alpha$ (dashed line), and $\alpha+\alpha$ (dotted line) scattering.

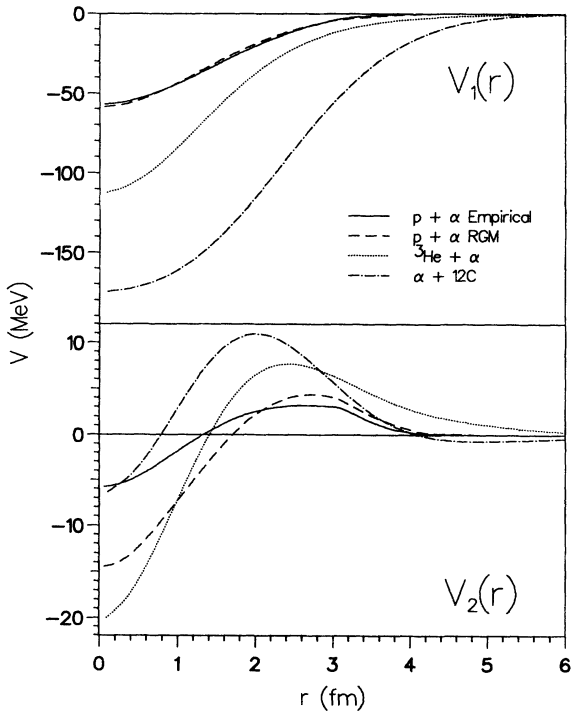


FIG. 8. The potentials $V_1(r)$ and $V_2(r)$, as described in the text for the cases $p+\alpha$ coupled channel RGM (solid line), $p$ + $\alpha$ empirical phase shifts (dashed line), $^3$He + $\alpha$ (dotted line), and $\alpha+^{12}$C (dash-dotted line).

TABLE II. Volume integrals $J$ (MeV fm$^3$), and the rms radii $\langle r^2\rangle^{1/2}$ (fm) for the even-parity potential, the odd-parity potential, and the parity-independent term $V_1(r)$ determined by inversion from the subthreshold RGM phase shifts of either LTK1 or LKT2.

| | Odd parity | | Even parity | | $V_1(r)$ | |
|---|---|---|---|---|---|---|
| | LTK1 | LKT2 | LTK1 | LKT2 | LTK1 | LKT2 |
| Central potential | | | | | | |
| $J$ | 639.0 | 629.0 | 298.0 | 298.0 | 469.0 | 463.0 |
| $\langle r^2\rangle^{1/2}$ | 3.26 | 3.25 | 2.19 | 2.19 | 2.96 | 2.94 |
| Spin-orbit potential | | | | | | |
| $J$ | 8.34 | 4.31 | 1.15 | 0.611 | - | - |
| $\langle r^2\rangle^{1/2}$ | 2.28 | 2.31 | 2.36 | 2.33 | - | - |

potential between the models LTK1 and LKT2. The volume integrals for the odd- and even-parity potentials are very close to the values derived from fitting $p+\alpha$ RGM phase shifts, particularly for the single-channel RGM, although, not surprisingly in the present case, the rms radii are larger. The volume integrals for the spin-orbit potentials, as expected, show a large dependence upon which RGM model is used.

## VI. CONCLUSIONS

A method has been introduced to allow the determination of a potential by inversion from both the subthreshold phase shifts and a chosen set of bound state energies. That is, a local potential can be determined for both the positive and negative energy regions. The procedure has been incorporated within the IP inversion program IMAGO. Low-energy resonance states are treated almost identically to the bound states, so that resonance energies can also be directly fitted by the new procedure. This forms an important addition to the IP procedure for the positive energy region since the original method may fail in an energy region containing narrow resonances.

The new method has been applied to determine a parity-dependent local potential from both low-energy $^3$He + $\alpha$ phase shifts and bound state energies in $^7$Be, calculated by the single-channel RGM. In the subthreshold energy region bound and resonance states exist only for odd-$l$ values, but the potential uncertainties are reduced by including these energies within the inversion, particularly for the very small spin-orbit potential. The even-parity potential is derived from the phase shifts alone and $D$-wave, as well to some extent $G$-wave, phase shifts are shown to be necessary to define the shape of this potential, confirming a suggestion of Liu *et al.* [5]. The existence of a parity-dependent potential, though not the precise radial shape, had already been established for this system. Contrary to the previous calculations of the $^3$He + $\alpha$ potential, the results found here show the even-parity potential to have a much smaller rms radius then the odd-parity potential, with the latter having a smaller depth at the nuclear center. The resulting parity-dependent potential is then strikingly similar to the potential found underlying both empirical and RGM subthreshold $p$ + $\alpha$ phase shifts. In the $^3$He + $\alpha$ case, the potentials are very nearly energy independent, except for the very small even-parity spin-orbit potential whose magnitude increases steadily with energy.

The shape of the parity dependence underlying the empirical phase shifts is less well determined, since a well-established local potential is obtained only for the odd-$l$ values. Whilst the $S$-wave phase shifts alone can be reproduced with a wide range of potential shapes, the ill-determined $D$- and $G$-wave phase shifts can only partially restrict the possible form of the even-parity potential. Forcing an energy continuity in the potential to ensure reasonable predictions are obtained at higher energies for the established $G_{7/2}$ resonance requires the even-parity to have a significantly smaller rms radius than the odd-parity potential. Hence inversion of the empirical phase shifts provide some support for the potential determined by inversion of RGM results.

It is now important to evaluate the parity-dependent potentials derived here in calculations of the $^3$He$(\alpha,\gamma)^7$Be capture reaction, following the suggestion that the most appropriate local potential for certain macroscopic reaction calculations [8] is one which can reproduce both bound state and phase shifts. At present, calculations are in progress to apply the potential local-equivalent to the RGM phase shifts in calculations of the astrophysical $S$ factor. The calculation of this factor is strongly dependent on the wave function of the $S$ wave [5], but requires an accurate calculation of the complete parity-dependent potential.

The possibility of an underlying energy dependence is a major problem when fitting data over a wide range of energies, particularly in the present case where the energy range extends to negative values. One signature of this energy dependence occurs where accurate inversion necessarily entails the introduction of long-range potential oscillations. Using the IP procedure, particularly with a parametrized form for the phase shifts, this energy dependence is easy to investigate. However, there is then an inevitable compromise between the approximate fitting of the phase shifts over a wide energy range and the accurate fitting of phase shifts with an energy-dependent potential. Which of the two choices is appropriate is likely to be determined by the subsequent use made of the potential. The approximate energy-independent potential is probably more useful for input into other structure models or reaction calculations, but the energy-dependent potential is more suitable for interpreting the implied systematics.

## ACKNOWLEDGMENTS

I am very grateful to Dr. Quincy Liu for patiently answering my numerous queries about the RGM calculations, to Dr. Ray Mackintosh for many helpful comments on the script, and also to the Science and Engineering council of the UK for support under Grant No. GR/H00895.

[1] Q.K.K. Liu, H. Kanada, and Y.C. Tang, Phys. Rev. C **23**, 645 (1981).
[2] H. Walliser, H. Kanada, and Y.C. Tang, Nucl. Phys. **A419**, 133 (1984).
[3] T. Kajino and A. Arima, Phys. Rev. Lett. **52**, 739 (1984).
[4] T. Mertelmeier and H.M. Hofman, Nucl. Phys. **A459**, 387 (1986).
[5] Q.K.K. Liu, H. Kanada, and Y.C. Tang, Phys. Rev. C **33**, 1561 (1986).
[6] B. Buck, R.A. Baldock, and J.A. Rubio, J. Phys. G **11**, L11 (1985).
[7] P. Mohr, H. Abele, R. Zweibel, G. Staudt, H. Krauss, H. Oberhummer, A. Denker, J.W. Hammer, and G. Wolf, Phys. Rev. C **48**, 1420 (1993).
[8] D. Baye and P. Descouvemont, Ann. Phys. (N.Y.) **165**, 115 (1985).
[9] S.G. Cooper and R.S. Mackintosh, Inverse Problems **5**, 707 (1989).
[10] S.G. Cooper and R.S. Mackintosh, Users manual for IMAGO, Report No. OUPD9201, 1992.
[11] Q.K.K. Liu, Y.C. Tang, and H. Kanada, Phys. Rev. C **41**, 1401 (1990).
[12] R.J. Spiger and T.A. Tombrello, Phys. Rev. **163**, 964 (1967).
[13] W.R. Boykin, S.D. Baker, and D.M. Hardy, Nucl. Phys. **A195**, 241 (1972).
[14] D.M Hardy, R.J. Spiger, S.D. Baker, Y.S. Chen, and T.A. Tombrello, Nucl. Phys. **A195**, 250 (1972).
[15] Y.W. Lui, O. Karban, A.K. Basak, C.O. Blyth, J.M. Nelson, and S. Roman, Nucl. Phys. **A297**, 189 (1978).
[16] W. Fetscher, E. Seibt, and Ch. Weddigen, Nucl. Phys. **A216**, 47 (1973).
[17] V.V. Ostashko and A.M Yasnogorodskii, Yad. Fiz. **50**, 656 (1989) [Sov. J. Nucl. Phys. **50**, 407 (1989)].
[18] Y.C. Tang, M. LeMere, and D.R. Thomson, Phys. Rep. **47**, 167 (1978).
[19] S.G. Cooper and R.S. Mackintosh, Nucl. Phys. **A517**, 285 (1990).
[20] S.G. Cooper and R.S. Mackintosh, Phys. Rev. C **43**, 1001 (1991).
[21] S.G. Cooper, R.S. Mackintosh, A. Csótó, and R.G. Lovas, Open University Report No. OUPD9314, 1993.
[22] B. Buck and J.A. Rubio, J. Phys. G **10**, L209 (1987).
[23] R.S. Mackintosh and S.G. Cooper, Phys. Rev. C **47**, 1716 (1993).
[24] P.D. Kunz, Computer code DWUCK, University of Colarado, 1978.
[25] J. Comfort, Extended version of DWUCK, University of Pittsburgh, unpublished, 1979.
[26] S.G. Cooper, R. Huby, and J.R. Mines, J. Phys. G **8**, 559 (1982).
[27] H. Kanada, T. Kaneko, and Y.C. Tang, Nucl. Phys. **A380**, 87 (1982).
[28] R.D. Furber, R.E. Brown, G.L. Peterson, D. R. Thompson, and Y.C. Tang, Phys. Rev. C **25**, 23 (1982).
[29] Y.C. Tang, E. Schmid, and K. Wildermuth, Phys. Rev. **131**, 2631 (1963).
[30] Q.K.K. Liu (private communication).
[31] Q.K.K. Liu, Nucl. Phys. **A550**, 263 (1992).
[32] B. Buck, H. Friedrich, and C. Wheatley, Nucl. Phys. **A275**, 246 (1977).